Hyperfine-structure intervals and isotope shifts in the $3p^4 4s\,^4P_J \rightarrow 3p^4 4p\,^4D_{J'}$ fine-structure multiplet of atomic chlorine by diode laser spectroscopy

D. A. Tate and J. P. Walton
Department of Physics and Astronomy, Colby College, Waterville, Maine 04901
(Received 10 August 1998; revised manuscript received 19 October 1998)

We have measured hyperfine-structure splittings and isotope shifts in the $4s\,^4P_J \rightarrow 4p\,^4D_{J'}$ multiplet in atomic chlorine using Doppler-free saturated absorption spectroscopy with an external cavity diode laser. Spectra of seven of the eight components of this multiplet, which have wavelengths between 798 and 859 nm, were obtained. Values for the magnetic dipole and electric quadrupole hyperfine-structure constants of the $^4P_{1/2-5/2}$ and $^4D_{1/2-7/2}$ states in both ^{35}Cl and ^{37}Cl were found, and the isotope shifts of the seven transitions studied were measured. The data were also analyzed in an attempt to extract values for magnetic octupole coupling constants for some of the levels investigated, but these were found to be zero at the level of the experimental uncertainty of our measurements. [S1050-2947(99)07702-1]

PACS number(s): 32.10.Fn, 32.30.Jc

I. INTRODUCTION

Atomic chlorine is an astrophysically important free radical which has two stable isotopes, ^{35}Cl (75.77% abundance, nuclear spin $I=\frac{3}{2}$) and ^{37}Cl (24.23% abundance, $I=\frac{3}{2}$). In addition, there is one long-lived radioactive isotope, ^{36}Cl, which has a half-life of 301 000 years and $I=2$. Though there have been many studies of the optical spectrum of atomic chlorine [1–4] made using grating spectrometers, the only experiments to measure hyperfine structure (hfs) intervals and isotope shifts in this species have been electron paramagnetic resonance investigations of the $^2P_{3/2}$ and $^2P_{1/2}$ states of the $3p^5$ ground configuration [5–7], and two studies of the $^2P_{3/2} \rightarrow {}^2P_{1/2}$ transition at 11.3 μm using a lead-salt diode laser [8,9].

In the present paper we report on the measurement of the hfs coupling constants of upper and lower states in the $3p^4 4s\,^4P_J \rightarrow 3p^4 4p\,^4D_{J'}$ fine-structure multiplet for ^{35}Cl and ^{37}Cl, and also isotope shifts for these transitions between the spectra of the two stable isotopes in seven of the eight members of this multiplet. This is the first time, to our knowledge, that high-resolution laser spectroscopy has been performed on excited states of atomic chlorine.

Excited states of atomic chlorine were generated from molecular chlorine using a microwave discharge. Spectra of the transitions were obtained using a tunable external cavity diode laser. The Doppler-free spectra were fitted to obtain the natural linewidths, hfs coupling constants for the upper and lower states of both stable isotopes, and the isotope shifts of the transition.

II. EXPERIMENTAL METHOD

The experimental apparatus used in this work is essentially the same as that used in a previous study of the hfs of atomic fluorine [10], so its description here will be brief. The apparatus is shown schematically in Fig. 1. A commercially available diode laser was mounted in a home-made temperature-stabilized external cavity [11]. One end of the cavity was formed by a 1200-line/mm blazed grating mounted on a commercial mirror mount; a thin piezoelectric disk mounted behind one of the adjustment screws allowed for fine tuning of the laser frequency. The laser frequency was scanned with a sawtooth voltage ramp applied to the piezoelectric disk, which enabled us to scan over a range of a few gigahertz. In addition to the output beam from the grating, four other beams were split out of the cavity using an uncoated glass plate. The output beam from the grating had a power of a few milliwatts, and a spectral linewidth of order 1 MHz. The wide spectral region covered by the chlorine transitions necessitated the use of several different laser diodes in the external cavity. For the $^4P_{3/2} \rightarrow {}^4D_{1/2}$ (vacuum wavelength 819.7 nm), $^4P_{5/2} \rightarrow {}^4D_{5/2}$ (821.4 nm), $^4P_{3/2} \rightarrow {}^4D_{3/2}$ (833.5 nm) $^4P_{5/2} \rightarrow {}^4D_{7/2}$ (837.8 nm), and $^4P_{1/2}$

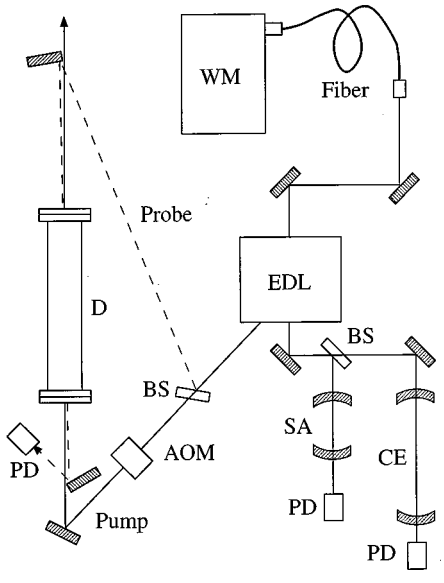

FIG. 1. Experimental apparatus for saturated absorption spectroscopy of chlorine: EDL, external cavity diode laser; PD, photodiode; SA, 2-GHz confocal spectrum analyzer; CE, 150-MHz confocal étalon; BS, beam splitter; AOM, acousto-optic modulator; *D*, microwave discharge tube; WM, wavemeter.

$\rightarrow {}^4D_{1/2}$ (843.1 nm) transitions, two different Sharp LT015 diodes were used, and for the ${}^4P_{1/2} \rightarrow {}^4D_{3/2}$ (857.8 nm) and ${}^4P_{3/2} \rightarrow {}^4D_{5/2}$ (858.8 nm) transitions, a SDL-5401 diode was used. We also attempted to obtain spectra of the ${}^4P_{5/2} \rightarrow {}^4D_{3/2}$ transition at 798.3 nm using a Sharp LT025 diode; however, the very weak absorption of the laser at this wavelength prevented us from obtaining Doppler-free spectra of this transition.

The main beam from the laser grating was used for the chlorine-saturated absorption spectrometer. The Doppler-free absorption signal was observed using standard saturated absorption techniques with an acousto-optic modulator (AOM) and lock-in amplifier. An uncoated glass window split off a few percent of the laser power for the probe beam. The pump beam power was sinusoidally ''chopped'' at 40 kHz with a 50% duty factor by modulation of the 47.98-MHz AOM drive signal. The probe beam was detected using a photodiode, and the Doppler-free signal was recovered by the lock-in amplifier using the AOM chopping frequency as reference. One of the beams from the laser intracavity beam splitter was used to monitor the laser mode structure using a 2-GHz confocal étalon and also to calibrate the frequency scan using a temperature-stabilized 150.127 ± 0.022-MHz free spectral range confocal étalon. The laser was tuned close to the appropriate wavelength of the $3p^4 4s\,{}^4P_J \rightarrow 3p^4 4p\,{}^4D_{J'}$ transitions [12] using a commercial wavemeter.

Excited chlorine atoms are generated from either neat Cl_2 or a dilute mix of Cl_2 in He in a low-pressure (0.02–0.2 torr) microwave discharge. The discharge system was configured so that gas was pumped through a half-inch diameter alumina tube from the gas bottle and regulators to the pump. High-quality quartz windows were o-ring sealed onto the vacuum system so as to allow the laser beams to pass longitudinally through the 6-inch-long discharge region. A McCarroll-type microwave cavity was attached to the outside of the alumina tube [13]; up to 100 W of microwave power at 2.45 GHz was coupled into the cavity by a coaxial cable. The alumina tube was cooled using compressed air. Under these conditions of pressure and microwave power, the minimum laser absorption was 2% for the ${}^4P_{5/2} \rightarrow {}^4D_{3/2}$ transition (too weak to obtain Doppler-free spectra); more typically the absorption was 30–40 % using neat Cl_2, but for the ${}^4P_{5/2} \rightarrow {}^4D_{7/2}$ transition, the absorption was in excess of 95% using neat Cl_2 at the lowest pressures and microwave powers at which a discharge could be maintained, necessitating our use of a 5% (by pressure) mix of Cl_2 in He.

The spectra were acquired using a digitizing oscilloscope and transferred to a PC. Many spectra were taken of each transition at various laser powers, microwave powers, and pressures so that the zero pressure and zero power widths and splittings could be determined. The raw data were then analyzed using a commercial software package. The typical analysis procedure involved linearizing the spectra using the étalon fringes, and then fitting the Voigt profiles to obtain line centers and homogeneous widths, and any Gaussian background features due to collisions, as described below.

III. RESULTS AND DISCUSSION

A term diagram of the $3p^4 4s\,{}^4P_J \rightarrow 3p^4 4p\,{}^4D_{J'}$ fine-structure multiplet, showing level energies with respect to the $2p^5\,{}^2P_{3/2}$ state and vacuum transition wavelengths obtained from tables [12], is given in Fig. 2.

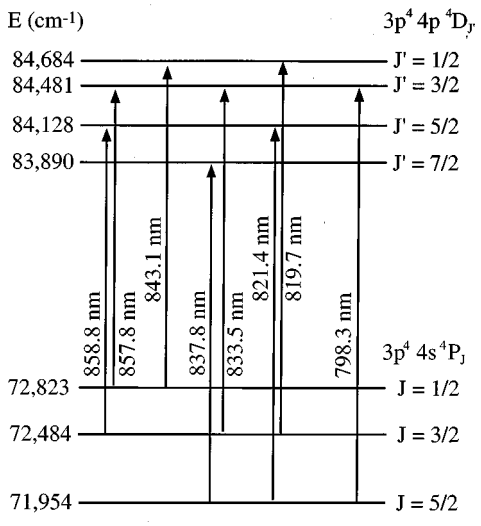

FIG. 2. Partial term diagram of Cl showing the transitions investigated in this work. Also given are the energies of the upper and lower states, and the vacuum wavelengths of the transitions.

At the temperatures present in the microwave discharge, Doppler broadening completely obscures the hfs splittings and isotope shifts in the $4s\,{}^4P_J \rightarrow 4p\,{}^4D_{J'}$ multiplet, as can be seen in Fig. 3, which shows the ${}^4P_{5/2} \rightarrow {}^4D_{5/2}$ transition at 821.4 nm. Figure 3(a) shows the Doppler-limited spectrum, while Fig. 3(b) shows the saturated absorption spectrum on the same frequency scale. These spectra were taken at a pressure of 120 mtorr and a microwave power of 90 W, the laser power being 2 mW. The hfs of this transition extends over some 2.3 GHz, the greatest spectral range of any member of the fine-structure multiplet with the exception of the ${}^4P_{5/2} \rightarrow {}^4D_{7/2}$ transition. It is also one of the most complex, having ten hyperfine transitions per isotope, plus a number of crossover resonances which result from the saturated absorption technique. As can be seen in Fig. 3(b), the hyperfine multiplets of ^{35}Cl and ^{37}Cl overlap, as they do in the six other members of the fine-structure multiplet which we studied. Fortunately, since both isotopes have $I = \frac{3}{2}$, their hyperfine spectra are similar, differing only in the isotope shift, the frequency intervals (due to different hf coupling constants), and amplitudes (due to the different isotopic abundances).

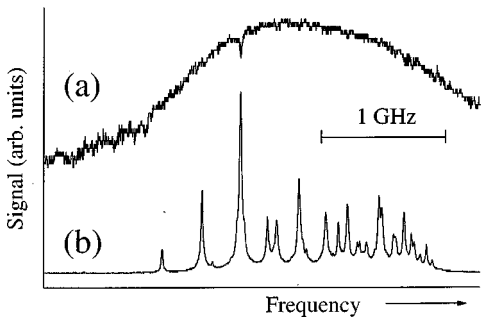

FIG. 3. Doppler-limited (a) and Doppler-free (b) spectra of the ${}^4P_{5/2} \rightarrow {}^4D_{5/2}$ transition at 821.4 nm. These spectra were obtained at a pressure of 0.12 torr and a microwave power of 90 W. The laser power was 2 mW.

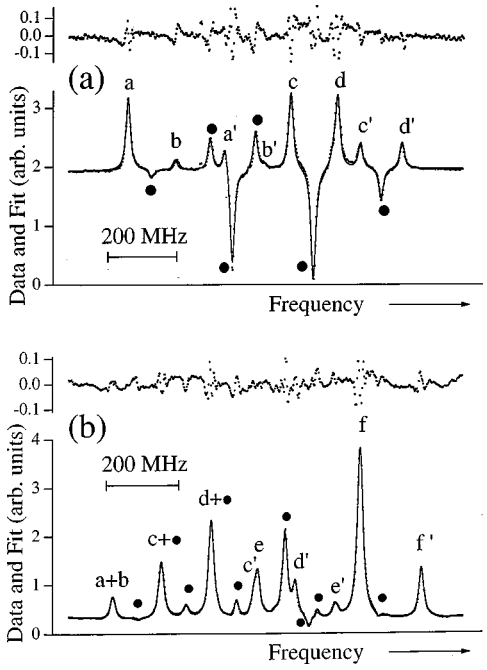

FIG. 4. Doppler-free spectra of the transitions originating in the $^4P_{1/2}$ state: $^4P_{1/2}\rightarrow{}^4D_{1/2}$ at 843.1 nm (a); and $^4P_{1/2}\rightarrow{}^4D_{3/2}$ at 857.8 nm (b). The dots are the data, the line is the result of the fit, and residuals (data minus fit) shown above the spectra. The vertical axis for the residuals has the same scale as that for the spectra. The individual $F\rightarrow F'$ components are identified by letter according to the scheme shown in Fig. 5(a) for $^4P_{1/2}\rightarrow{}^4D_{1/2}$ and Fig. 5(b) for $^4P_{1/2}\rightarrow{}^4D_{3/2}$. The unprimed letters are the transitions due to ^{35}Cl, while the primed letters identify the corresponding transitions in ^{37}Cl. Crossovers are identified by the • symbol.

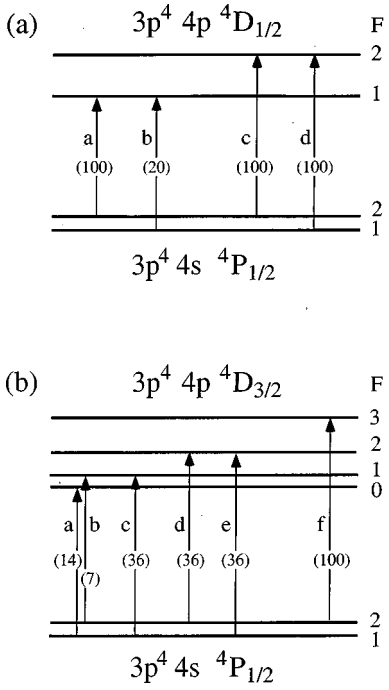

FIG. 5. Diagrams of the hfs of the upper and lower levels of the two fine-structure transitions shown in Fig. 4. (a) identifies the hf transitions in $^4P_{1/2}\rightarrow{}^4D_{1/2}$, and (b) identifies the hf transitions in $^4P_{1/2}\rightarrow{}^4D_{3/2}$. Letters (*a*, *b*, *c*, etc.) represent the F values connected by a particular hf component: for instance, in (a), *a* represents the $F=2\rightarrow F'=1$ component, which appears in the Doppler-free spectrum in Fig. 4(a) as the peak identified by the letter *a* for ^{35}Cl, and by a' for ^{37}Cl. The numbers in brackets on the individual transitions are their calculated relative intensities within the multiplet.

But for this simplification, it is doubtful that we could have identified the spectral components without having to resort to isotopically enriched chlorine samples.

The data analysis of the spectrum of a particular $^4P_J\rightarrow{}^4D_{J'}$ transition was carried out as follows. The raw spectra were linearized using the 150-MHz étalon fringes, and smoothed to give one data point for every 2-MHz frequency interval. Peaks were tentatively identified (in terms of the F values of their lower and upper states) using calculated relative intensities obtained from tables. This process was somewhat tedious given the complexity of some of the spectra, but was aided by the presence of the crossover resonances (though these sometimes obscured real transitions of the less abundant isotope) and the fact that the ^{35}Cl and ^{37}Cl spectra are basically similar. Once a sufficient number of components were identified, frequency intervals between peaks were used to obtain tentative magnetic dipole (A) and electric quadrupole (B) coupling constants, and also a value for the isotope shift of the transition. Usually, our first set of values for these parameters was reasonably correct, given the corroboration of taking the ratios of the A and B values for the two isotopes, and comparing them with the ratios of these quantities for the $3p^5\,{}^2P_{1/2}$ and $^2P_{3/2}$ states of the ground configuration [7]. A ''stick diagram'' of the spectrum, using the initial guesses for the hf coupling constants and isotope shift, was then made. The diagram included all the allowed transitions of both isotopes, and the expected crossovers, which have frequencies which are midway between pairs of transitions which share either a lower or an upper state (the latter crossovers were usually inverted in the experimental spectra). The relative intensities of the components were taken from tables, and the relative intensities of the ^{37}Cl components set to 32% of the corresponding ^{35}Cl transition (the crossover amplitudes were arbitrarily set to the arithmetic mean of the intensities of their parent transitions). The stick diagram was then compared with the real spectrum, and if necessary, refinements made to the initial guesses for isotope shift and coupling constants. In the course of this comparison, crossovers not manifesting themselves were identified (to be excluded from the fit), and unexpected crossovers identified (i.e., crossovers which share neither a lower nor an upper state, but appearing due to collisional redistribution of population between closely spaced states). Identification of the spectral features progressed more rapidly once other fine-structure transitions sharing upper or lower states had been fitted.

To obtain an estimate for the residual Doppler broadening present in the saturated absorption spectra, we fitted some of the Doppler-limited spectra to a sum of Gaussians (one for each real hf transition in each isotope) with relative frequency positions determined by the method described above, and relative intensities based on tabulated values and the isotopic abundance ratio. This was done for the $^4P_{3/2}\rightarrow{}^4D_{1/2}$ (819.7 nm) and the $^4P_{5/2}\rightarrow{}^4D_{5/2}$ (821.4 nm) transitions, and gave values for the Gaussian full width at half maximum (FWHM) of 1158 ± 12 MHz, implying a tempera-

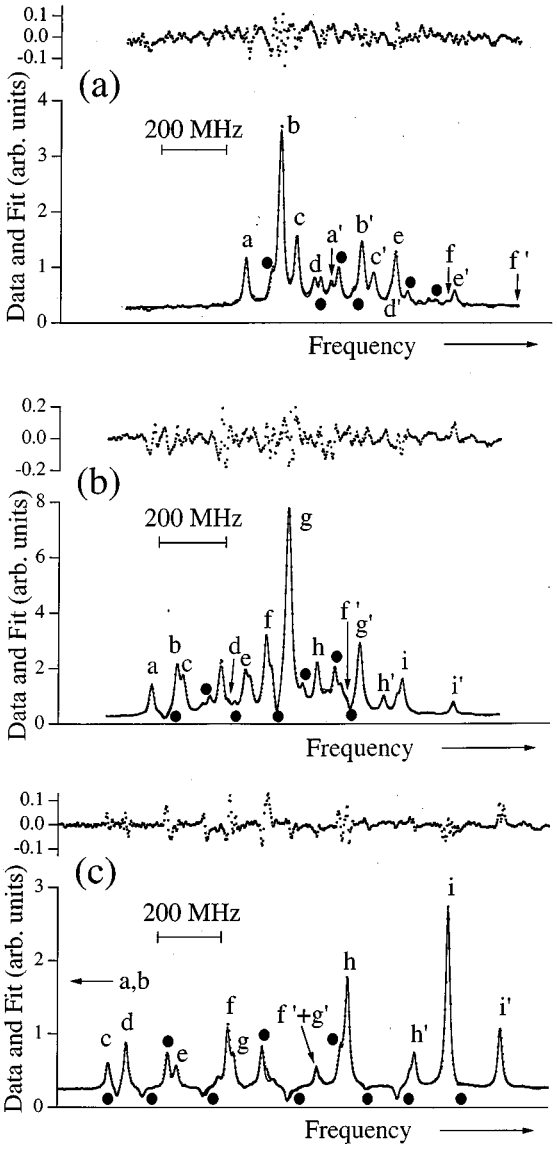

FIG. 6. Doppler-free spectra of the transitions originating in the $^4P_{3/2}$ state: $^4P_{3/2}\rightarrow{}^4D_{1/2}$ at 819.7 nm (a); $^4P_{3/2}\rightarrow{}^4D_{3/2}$ at 833.5 nm (b); and $^4P_{3/2}\rightarrow{}^4D_{5/2}$ at 858.8 nm (c).

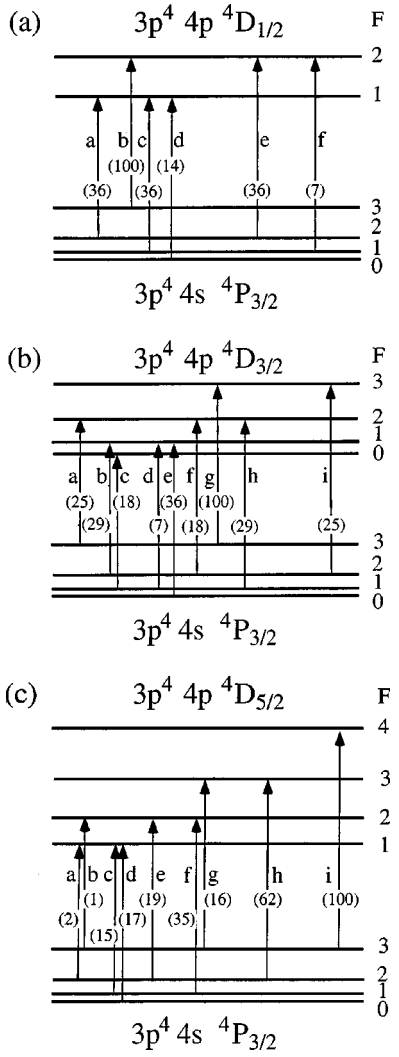

FIG. 7. Diagrams of the hfs of the upper and lower levels of the three fine-structure transitions shown in Fig. 6: $^4P_{3/2}\rightarrow{}^4D_{1/2}$ (a); $^4P_{3/2}\rightarrow{}^4D_{3/2}$ (b); and $^4P_{3/2}\rightarrow{}^4D_{5/2}$ (c).

ture in the discharge of $T=713\pm16$ K. The residual Doppler broadening of our saturated absorption spectra, calculated using the Doppler width and the pump-probe crossing angle, was thus 3.6-MHz FWHM, a parameter that was fixed in our fits as described below. We note, however, that the fitted Lorentzian widths were relatively insensitive to the Gaussian width.

The Doppler-free spectra were then fitted using the initial estimates for the hf coupling constants for the upper and lower states and the isotope shift of the transition obtained by the method described above. The spectra were fitted assuming that the spectral features were Voigt profiles with identical Lorentzian and Gaussian widths but different amplitudes, and whose positions (for each isotope) were determined only by the center of gravity of each multiplet, and the magnetic dipole and electric quadrupole hf coupling parameters of the upper and lower states. For instance, in the spectrum shown in Fig. 3(b), the positions of some 32 relatively obvious spectral features (including small bumps between, and shoulders on, some of the larger peaks) were determined by just ten parameters: the center of gravity, and the A and B values for the $^4P_{5/2}$ and $^4D_{5/2}$ states, of each isotope. In the actual fit of this spectrum, 18 spectral features in each isotope were fitted (ten real transitions and eight crossovers). These 18 features were all identified in ^{35}Cl using the stick diagram, but all are not obvious in ^{37}Cl, some being hidden by larger features in ^{35}Cl. Initially, 19 floating parameters were used in the fit to determine the amplitudes of all the 36 spectral features: 18 amplitudes in each isotope, plus a parameter representing the isotope abundance ratio (i.e., the peaks in ^{37}Cl were assumed to be lower in amplitude than their counterparts in ^{35}Cl by a factor equal to the isotope abundance ratio). When fitted thus, the abundance ratio determined from the fits was found to be $(34\pm4)\%$, compared with an expected value of 31.98%. Generally, the fits in which the isotope abundance ratio was floated gave higher values than the 31.98% expected, presumably because in the ^{37}Cl wing of the Doppler profile the linear absorption of the pump and probe beams was weaker than in the ^{35}Cl wing. In some fits we fixed the isotope ratio to this value with no significant increase in the χ^2 value for the fit or the fitted

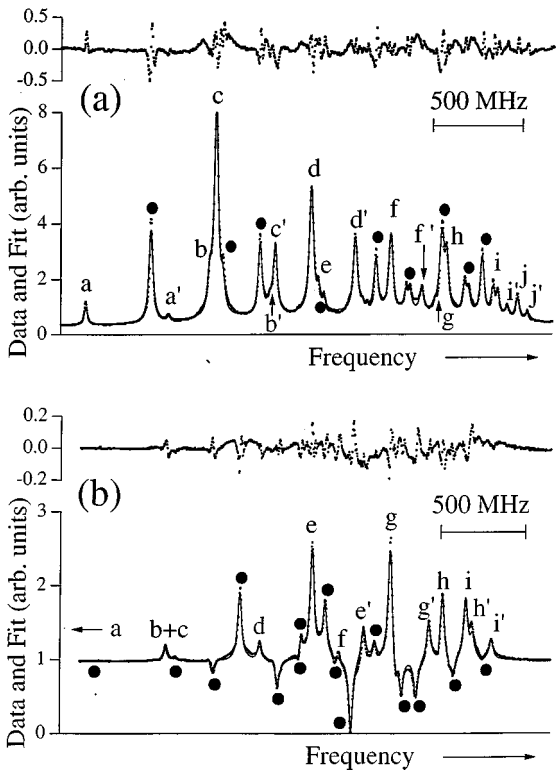

FIG. 8. Doppler-free spectra of the transitions originating in the $^4P_{5/2}$ state: $^4P_{5/2}\rightarrow{}^4D_{5/2}$ at 821.4 nm (a); and $^4P_{5/2}\rightarrow{}^4D_{7/2}$ at 837.8 nm (b).

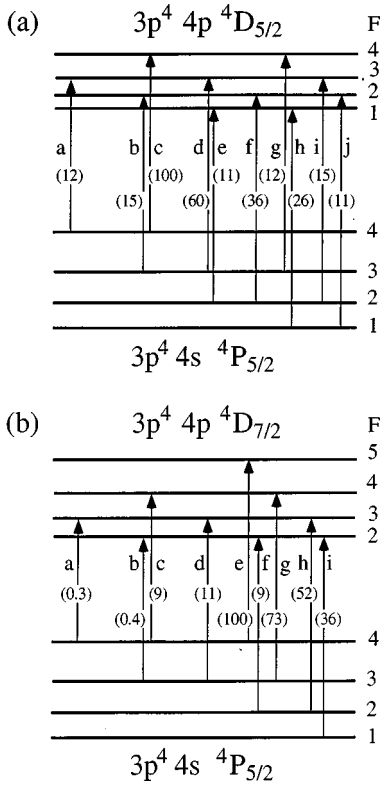

FIG. 9. Diagrams of the hfs of the upper and lower levels of the two fine-structure transitions shown in Fig. 8: $^4P_{5/2}\rightarrow{}^4D_{5/2}$ (a); and $^4P_{5/2}\rightarrow{}^4D_{7/2}$ (b).

values of the hfs coupling constants or centers of gravity. The Gaussian width was fixed at that determined by the pump-probe beam crossing geometry, but the Lorentzian width was floated. The fits also floated the background offset and a linear background slope, and in some cases a single Gaussian pedestal was included with floated position, width, and amplitude. Hence, to fit the spectrum of Fig. 3(b), a total of 35 free parameters was used: eight hf coupling constants (four for each isotope), two centers of gravity (one for each isotope), 18 amplitudes, the isotope abundance ratio, Lorentzian width, background offset and slope, and three parameters for the Gaussian pedestal. In some spectra, where the isotope ratio was fixed and no pedestal was apparent, this was reduced to 31.

Obviously, the number of floated parameters varied with the fine-structure component being fitted, depending on the number of hf components and crossovers observed, and also on whether the electric quadrupole moment of the upper or lower state was zero or not. The most complex spectrum to fit was the $^4P_{5/2}\rightarrow{}^4D_{7/2}$ transition at 837.8 nm, which required a 38-parameter fit (34 parameters if the isotope abundance ratio was fixed and no Gaussian pedestal) due to the unusually large number of crossovers. In the fit of this transition, seven real hf components of non-negligible amplitude and 15 crossovers were included for each isotope. The spectrum which required the fewest parameters to fit was the $^4P_{1/2}\rightarrow{}^4D_{1/2}$ transition at 843.1 nm, in which $B=0$ for both the upper and lower states. This spectrum required a maximum of 22 parameters to fit, 18 if the isotope ratio was fixed and the pedestal not manifested. Finally, in some of the spectra, there were coincidences in the positions of two (or even three) real hyperfine transitions, or a coincidence between a real transition and a crossover. Such coincidences, if they occurred between features of the same isotope, led to anomalous intensity ratios for the real transitions (some becoming very small, or even negative, the others very large) in the fit. In these cases, the real hf components in question were fitted with their intensity relative to some nonobscured feature fixed to its theoretical value, while any coincident crossover was allowed to float in amplitude.

The results of these fits are shown in Figs. 4, 6, and 8. Figure 4 shows the transitions originating in the $^4P_{1/2}$ state: the $^4P_{1/2}\rightarrow{}^4D_{1/2}$ at 843.1 nm [Fig. 4(a)] and $^4P_{1/2}\rightarrow{}^4D_{3/2}$ at 857.8 nm [Fig. 4(b)] transitions. The dots are the data, the line is the result of the fit, and residuals (difference between the data and the fit) shown on a separate scale above the spectra. In Fig. 5 we show the positions of the upper and lower hf states (for one isotope only), the allowed hf transitions (identified by letter: *a*, *b*, *c*, etc.), and their expected relative intensities, for the $^4P_{1/2}\rightarrow{}^4D_{1/2}$ transition [Fig. 5(a)] and the $^4P_{1/2}\rightarrow{}^4D_{3/2}$ transition [Fig. 5(b)]. The level spacings in Fig. 5 are inferred from the spectra in Fig. 4. In the spectrum shown in Fig. 4(a), the individual hf $F\rightarrow F'$ components are identified by the letter each is assigned in Fig. 5(a), and similarly the components in Fig. 4(b) are identified in Fig. 5(b). The unprimed letters are the features due to ^{35}Cl, the primed letters the corresponding features in the ^{37}Cl spectrum. Figure 6 shows transitions from $^4P_{3/2}$:$^4P_{3/2}\rightarrow{}^4D_{1/2}$ at 819.7 nm [Fig. 6(a)], $^4P_{3/2}\rightarrow{}^4D_{3/2}$ at 833.5 nm [Fig. 6(b)], and $^4P_{3/2}\rightarrow{}^4D_{5/2}$ at 858.8 nm [Fig. 6(c)]. The individual hf components in Figs. 6(a)–6(c) are identified in Figs. 7(a)–7(c), respectively. Figure 8 shows transitions

from $^4P_{5/2}$: $^4P_{5/2}\rightarrow{}^4D_{5/2}$ at 821.4 nm [Fig. 8(a)] and $^4P_{5/2}\rightarrow{}^4D_{7/2}$ at 837.8 nm [Fig. 8(b)]. The individual hf components in Figs. 8(a) and 8(b) are identified in Figs. 9(a) and 9(b), respectively. As noted above, the $^4P_{5/2}\rightarrow{}^4D_{3/2}$ transition at 798.3 nm was too weak for us to obtain spectra. Letters are omitted from the spectra shown in Figs. 4, 6, and 8 where a weak feature is obscured by another, stronger feature. Crossovers are indicated by the solid circle. In some cases, exceptionally weak features at the extreme high- and low-frequency wings of a multiplet are omitted from the spectra, for instance, at the low-frequency end of Figs. 6(c) and 8(b), and at the high-frequency end of Fig. 6(a), where the $F=1\rightarrow F'=2$ component in $^{37}\mathrm{Cl}\,(f')$ is not apparent in the data. As can be seen, the quality of the fits is very good considering the relatively small number of parameters which determines all the peak positions within a given multiplet. The maximum deviation of the fit from the data is of order 3% of the maximum peak amplitude in a given spectrum. Perhaps the only effect visible in the residuals of some of the spectra not allowed for in our fits are possible narrow (~30-MHz FWHM) Gaussian pedestals on some of the stronger peaks, for instance, in Fig. 8(a). (We were unable to include this effect in our fits due to the extra number of floating parameters this would introduce.)

The magnetic dipole and electric quadrupole hf coupling constants for both isotopes derived from these spectra are given in Table I in units of MHz. With two exceptions, each value of A and B is obtained from fitting the spectra of at least two, and sometimes three, different wavelengths. A number of Doppler-free spectra were obtained of each fine-structure component. The 819.7-, 821.4-, 833.5-, 837.8-, and 843.1-nm transitions were sufficient to give a complete set of A and B values, and at each of these wavelengths between 17 and 40 spectra were obtained. The 857.8- and 858.8-nm transitions confirmed some of our hf component assignments and hf coupling constants, and we took only seven and five spectra of these transitions, respectively. The mean values of A and B from different fine-structure components usually agreed within the standard deviations of their means, and the uncertainties shown in Table I are one standard deviation of the mean of the combined results. These standard deviations were obtained by statistical analysis of many sets of A and B values, each set being obtained from the fit of one spectrum. The values for A and B for the $^4D_{7/2}$ state could only be obtained from the $^4P_{5/2}\rightarrow{}^4D_{7/2}$ transition, in which the strong linear absorption in the discharge and the presence of strong, inverted, crossovers resulted in significantly larger error estimates.

TABLE I. Magnetic dipole hfs constants (A) and electric quadrupole hfs constants (B) for the $4s\,^4P_{1/2}$, $4s\,^4P_{3/2}$, $4s\,^4P_{5/2}$, $4p\,^4D_{1/2}$, $4p\,^4D_{3/2}$, $4p\,^4D_{5/2}$, and $4p\,^4D_{7/2}$ levels of ^{35}Cl and ^{37}Cl. The errors are one standard deviation of the mean, calculated from many sets of A and B values, each set being obtained from the fit of a single spectrum.

	^{35}Cl		^{37}Cl	
Level	A (MHz)	B (MHz)	A (MHz)	B (MHz)
$^4P_{1/2}$	67.0±0.9	0	57.0±0.4	0
$^4P_{3/2}$	101.1±0.2	47.3±0.3	84.5±0.5	37.6±1.2
$^4P_{5/2}$	299.6±0.2	−62.5±0.4	251.0±0.8	−52.7±1.3
$^4D_{1/2}$	227.5±0.2	0	189.1±0.5	0
$^4D_{3/2}$	138.2±0.2	2.6±0.2	115.1±0.1	2.1±0.4
$^4D_{5/2}$	170.3±0.2	−29.4±0.5	142.1±0.5	−23.6±0.5
$^4D_{7/2}$	160.2±0.4	−65.4±6.4	135.3±0.9	−58.3±6.3

In the fitting of the spectra described above, we assumed that only the magnetic dipole and electric quadrupole coupling constants (A and B, respectively) were significant, i.e., that the shift of a given F state from the unperturbed energy (that is, ignoring hfs) is given by

$$\Delta E_F=\frac{1}{2}AK+\frac{1}{4}B\,\frac{\frac{3}{2}K(K+1)-2I(I+1)J(J+1)}{I(2I-1)J(2J-1)}, \quad (1)$$

where $K=F(F+1)-J(J+1)-I(I+1)$. The position with respect to the multiplet center of gravity of a given $F\rightarrow F'$ component thus depends on the A and B values of the upper and lower states. However, both stable chlorine isotopes, having $I=\frac{3}{2}$, can exhibit a magnetic octupole effect in the hfs of states with $J>\frac{1}{2}$, which adds another term to Eq. (1):

$$\frac{5}{4}C\,\frac{K^3+4K^2+\frac{4}{5}K[-3I(I+1)J(J+1)+I(I+1)+J(J+1)+3]-4I(I+1)J(J+1)}{I(I-1)(2I-1)J(J-1)(2J-1)}, \quad (2)$$

where C is the magnetic octupole coupling constant [14]. The only state of Cl for which hfs measurements have been made from which a value of C can be obtained is $3p^5\,{}^2P_{3/2}$, for which $A=205.046\,87(3)$ MHz, $B=54.872\,90(6)$ MHz, and $C=-7.2(1.2)$ Hz for ^{35}Cl, and $A=170.686\,37(3)$ MHz, $B=43.245\,24(6)$ MHz, and $C=-5.5(1.2)$ Hz for ^{37}Cl [5–7].

Clearly, for the $3p^5\,{}^2P_{3/2}$ state, the effect on the hfs splittings of the magnetic octupole coupling constant is almost negligible compared with that of the magnetic dipole interaction. Indeed, it is unlikely that such a small effect will manifest itself in our optical spectra, given our resolution limit of ~1 MHz, and laser scan nonlinearities of the same order. In addition, we note that the dependence of C on the electron wave function, in common with A and B, is such that one expects its magnitude to decrease with increasing electronic excitation [14]. We did not, therefore, expect that our data would reveal values for C for the $4s\,^4P_J$ and $4p\,^4D_{J'}$ states. Nevertheless, we fitted our data including the effect of the magnetic octupole coupling constants of all up-

TABLE II. Experimental values of the isotope shifts (''Measured IS'') of the seven members of the $4s\,^4P_J \rightarrow 4p\,^4D_{J'}$ multiplet studied in this work. Also given are calculated values for the normal mass shift (NMS) and inferred values for the residual isotope shift (RIS) which is equal to measured IS minus NMS. The errors are one standard deviation of the mean, calculated from many isotope shift values, each isotope shift being obtained from the fit of a single spectrum.

Transition $J \rightarrow J'$	Wavelength (nm)	Measured IS (MHz)	NMS (MHz)	RIS (MHz)
$3/2 \rightarrow 1/2$	819.7	231.1 ± 0.2	310.0	-78.9
$5/2 \rightarrow 5/2$	821.4	228.7 ± 0.2	309.3	-80.6
$3/2 \rightarrow 3/2$	833.5	229.0 ± 0.2	304.8	-75.8
$5/2 \rightarrow 7/2$	837.8	214.5 ± 0.3	303.2	-88.7
$1/2 \rightarrow 1/2$	843.1	215.8 ± 0.2	301.4	-85.6
$1/2 \rightarrow 3/2$	857.8	212.9 ± 0.5	295.8	-82.9
$3/2 \rightarrow 5/2$	858.8	224.9 ± 0.5	295.8	-70.9

per and lower states with $J > \frac{1}{2}$ for all the transitions we investigated with the exception of $^4P_{5/2} \rightarrow {}^4D_{7/2}$. To reduce the number of parameters in the fits, we fixed the hf coupling constants of a given state for ^{37}Cl to a constant factor of the same coupling constant for ^{35}Cl. We obtained these constant factors from the hf coupling constants of the $3p^5\,{}^2P_{3/2}$ state given by Altan-Uslu, Code, and Harvey [7]. The factors are, respectively, $A(^{37}\mathrm{Cl}) = 0.832\,426 \times A(^{35}\mathrm{Cl})$, $B(^{37}\mathrm{Cl}) = 0.788\,098 \times B(^{35}\mathrm{Cl})$, and $C(^{37}\mathrm{Cl}) = 0.76 \times C(^{35}\mathrm{Cl})$. Our results given in Table I are reasonably consistent with these ratios of A and B for the two isotopes. When values of $A(^{37}\mathrm{Cl})/A(^{35}\mathrm{Cl})$ and $B(^{37}\mathrm{Cl})/B(^{35}\mathrm{Cl})$ are calculated along with their uncertainties from the data in Table I, four out of seven of the A ratios and three out of five of the B ratios agree with the values given above for the $2p^5\,{}^2P_{3/2}$ state, within one standard deviation. The remaining differences are all within 2σ. However, when we fitted the spectra including the magnetic octupole effect, the mean C values resulting from the fits were consistent with zero within the error limits (one standard deviation of the mean obtained from sets of individual C values, each value being obtained from the fit of one spectrum). We thus conclude that no meaningful values for the magnetic octupole coupling constants of the $4s\,^4P_{3/2-5/2}$ and $4s\,^4D_{3/2-5/2}$ states can be obtained from our spectra.

We also obtained values for the isotope shifts of the seven transitions studied, which are given in Table II, in units of MHz. The errors quoted are standard deviations of the means. (The standard deviations of the isotope shifts were calculated from the sets of isotope shift values obtained from fits of different data scans.) In all cases, the center of gravity of the ^{37}Cl hfs was about 220 MHz higher in frequency than that of ^{35}Cl, but the measured isotope shifts are all smaller than the calculated values of the normal mass shift (NMS) of about 300 MHz, also given in Table II. We have also derived values for the residual isotope shift (RIS), the sum of the specific mass shift (SMS), and the field shift (FS), from the measured isotope shifts and the calculated SMS values, which are given in the last column of Table II.

The relative amplitudes of the hf components of a multiplet whose intensities were allowed to float were all relatively close (within about 10%) to the theoretical ratios given in Figs. 4, 6, and 8, with the exception of some of the weak features in the low- and high-frequency wings of the spectra which were excessively attenuated by the large linear absorption of the laser in the discharge. As noted above, in those fits in which the isotope ratio was floated, the ratio came out to be within 4% of 34%, whereas the natural relative abundance ratio of the isotopes is 31.98%.

Lorentzian linewidths were also extracted from the data, either by extrapolation to zero pump laser power and zero pressure (the 819.7-, 833.5-, 837.8-, and 843.1-nm transitions), or just to zero pressure (821.4, 857.8, and 858.8 nm). There was no significant linewidth dependence on the microwave power, but this could not be fully investigated since the discharge was unstable at powers of below 60 W. The minimum FWHM Lorentzian widths observed were 14 ± 1 MHz for the $^4P_{3/2} \rightarrow {}^4D_{1/2}$ (819.7 nm), $^4P_{3/2} \rightarrow {}^4D_{3/2}$ (833.5 nm), $^4P_{1/2} \rightarrow {}^4D_{1/2}$ (843.1 nm), $^4P_{1/2} \rightarrow {}^4D_{3/2}$ (857.8 nm), and $^4P_{3/2} \rightarrow {}^4D_{5/2}$ (858.8 nm) transitions and 22 ± 2 MHz for the $^4P_{5/2} \rightarrow {}^4D_{5/2}$ (821.4 nm) and $^4P_{5/2} \rightarrow {}^4D_{7/2}$ (837.8 nm) transitions.

To our knowledge, the only direct measurement of radiative lifetimes in chlorine are those of Lawrence [15] using the phase-shift method and Schectman *et al.* [16] using the beam-foil method. Lawrence reports lifetime measurements for two vacuum ultraviolet (vuv) transitions: the $3p^4 4s\,{}^2P_{1/2} \rightarrow 3p^5\,{}^2P_{3/2}$ (1335 Å) and the $3p^4 4s\,{}^4P \rightarrow 3p^5\,{}^2P$ transition at 1390 Å (it is unclear whether this means the $3p^4 4s\,{}^4P_{5/2} \rightarrow 3p^5\,{}^2P_{3/2}$ or the $3p^4 4s\,{}^4P_{1/2} \rightarrow 3p^5\,{}^2P_{1/2}$ transition), for which the measured lifetimes were 2 ns ($\pm 15\%$) and 1.5 μs ($\pm 15\%$), respectively. Hence, the partial width due to the $3p^4 4s\,{}^4P$ state of any absorption or emission seems to be of order 100 kHz. Schectman *et al.* [16] measured lifetimes and oscillator strengths of several of the $3p^4 4s\,{}^2P \rightarrow 3p^5\,{}^2P$ resonance transitions in the vuv. Generally, the lifetimes of the visible transitions in chlorine have been found to be too long to be measured using the beam-foil technique [17]. Delalić *et al.* [17] have measured the lifetimes of a number of visible transitions in Cl using the high-frequency deflection technique. In particular, the lifetime of the $3p^4 5p\,{}^4D_{3/2} \rightarrow 3p^4 4s\,{}^4P_{3/2}$ radiative decay at 4380 Å was found to be 135 ± 15 ns, indicating a Lorentzian width of 1.2 MHz (the $3p^4 4s\,{}^4P \rightarrow 3p^4 4p\,{}^4D$ multiplet was not investigated by Delalić *et al.*). On the other hand, there have been numerous experimental and theoretical studies of oscillator strengths in Cl [2–4,16,18,19]. However, only Ojha and Hibbert [19] have calculated oscillator strengths for all allowed and forbidden decay transitions of the $4s\,{}^4P$ and $4p\,{}^4D$ states. From the f values given by Ojha and Hibbert, we have calculated the natural radiative linewidths of the $4s\,{}^4P \rightarrow 4p\,{}^4D$ transitions to be between 5 and 7 MHz. These linewidths are dominated by the $4p\,{}^4D \rightarrow 4s\,{}^4P$ radiative decay, though the $4p\,{}^4D \rightarrow 4s\,{}^2P$ decays are significant, and the radiative widths of the $4s\,{}^4P_{1/2}$, $4s\,{}^4P_{3/2}$, and $4s\,{}^4P_{5/2}$ states are 0.4, 1.5, and 0.04 MHz, respectively, based on Ojha and Hibbert's f values.

Clearly, our measured linewidths of 14 ± 1 and 22 ± 2 MHz are much greater than is to be expected from the theoretical f values, whose absolute accuracy is estimated to

be ±20% [19], based on the degree of agreement between the length-and velocity-gauge calculations. It is possible that some of the excess linewidth is due to microwave power effects. However, it is more likely that, even at the lowest pump intensities used in this experiment, we were still significantly saturating the transitions. We have calculated the saturation intensities of the eight components of the $4s\,^4P_J \rightarrow 4p\,^4D_{J'}$ fine-structure multiplet using the line strength values given by Wiese, Smith, and Glennon [12], and radiative linewidths derived from Ojha and Hibbert [19]. The effect of collisional quenching on the saturation intensities is difficult to estimate, since from our data we can only measure pressure broadening of the saturated absorption signals which is a measure of the sum of the upper and lower state relaxation rates. By using only the radiative relaxation rates, we are thus underestimating the saturation intensities, but they nevertheless give a useful parameter with which to compare the laser intensities we used in our experiment. The calculated saturation intensities (assuming negligible collisional quenching) vary from 0.3 and 1 μW/mm^2 for the $^4P_{5/2} \rightarrow {}^4D_{5/2}$ and $^4P_{5/2} \rightarrow {}^4D_{7/2}$ components, respectively, to 140 μW/mm^2 for the $^4P_{3/2} \rightarrow {}^4D_{1/2}$ component, and are between 6 and 20 μW/mm^2 for the other five fine-structure components. Typical pump laser beam intensities used in this experiment were in the range 1–10 mW/mm^2, and in those cases where we carried out an extrapolation to low laser intensities, the pump laser intensity was in the range of 10–400 μW/mm^2, with the probe laser beam being on the same order. As can be seen, even for the reduced intensities used to observe some of the transitions, the pump laser intensities were still greater than the calculated saturation intensities. The spectra obtained at higher intensities were therefore even more saturated. Further discussion is somewhat pointless since, as we have already noted, our calculated saturation intensities are underestimates. All that can be stated is that the intensities used in our experiments were at least several times greater than the minimum saturation intensities, and that our observed linewidths were several times greater than the calculated widths.

IV. CONCLUSION

We have obtained Doppler-free spectra of the $3p^4 4s\,^4P_J \rightarrow 3p^4 4p\,^4D_{J'}$ fine-structure multiplet of atomic chlorine. From these spectra, we have deduced values for the magnetic dipole and electric quadrupole hyperfine-structure coupling constants of the upper and lower states for both stable isotopes, and the isotope shifts of the transitions. To our knowledge, these are the first measurements of such parameters in an excited configuration of this atom. The A and B constants were found to be of the same order as those of the $3p^5\,^2P_{1/2}$ and $3p^5\,^2P_{3/2}$ states of the ground configuration obtained using electron paramagnetic resonance [5–7] and confirmed using mid-infrared diode laser spectroscopy [8,9]. An attempt was also made to extract values for the magnetic octupole hf coupling constants, but these were all found to be zero at the resolution offered by our spectra. The natural linewidths of the transitions were found to be three to five times larger than the values calculated from theoretical oscillator strengths [19], mostly due to unallowed-for laser power broadening, but quenching due to the high microwave power necessary to maintain the discharge probably also contributes to this excess width.

ACKNOWLEDGMENTS

We would like to thank Charlie Conover for many interesting discussions concerning this work. We also acknowledge assistance from Ryan Jennerich. Funding for these experiments has been provided by Colby College, the Research Corporation, a Maine EPSCoR grant (Grant No. MSTF 96-12N), and the NSF Academic Research Infrastructure Program (Grant No. PHY-9601638).

[1] C. J. Humphreys and E. Paul, J. Opt. Soc. Am. **49**, 1180 (1959), and references therein.
[2] P. Hey, Z. Phys. **157**, 79 (1959).
[3] E. W. Foster, Proc. Phys. Soc. London **80**, 882 (1962).
[4] R. D. Bengtson, M. H. Miller, D. W. Koopman, and T. D. Wilkerson, Phys. Rev. A **3**, 16 (1971).
[5] J. G. King and V. Jaccarino, Phys. Rev. **84**, 582 (1951).
[6] J. H. Holloway, B. B. Aubrey, and J. G. King, Proc. R. Soc. London **76**, 984 (1960).
[7] K. Altan-Uslu, R. F. Code, and J. S. M. Harvey, Can. J. Phys. **52**, 2135 (1974).
[8] P. B. Davies and D. K. Russell, Chem. Phys. Lett. **67**, 440 (1979).
[9] A. C. Stanton, Chem. Phys. Lett. **122**, 385 (1985).
[10] D. A. Tate and D. N. Aturaliye, Phys. Rev. A **56**, 1844 (1997).
[11] K. B. MacAdam, A. Steinbach, and C. Wieman, Am. J. Phys. **60**, 1098 (1992).
[12] W. L. Wiese, M. W. Smith, and B. M. Glennon, *Atomic Transition Probabilities (Volume II Sodium Through Calcium)* (NBS, Washington, D.C., 1966).
[13] F. C. Fehsenfeld, K. M. Evenson, and H. P. Broida, Rev. Sci. Instrum. **36**, 294 (1965).
[14] N. F. Ramsay, *Molecular Beams* (Oxford University Press, Oxford, 1956).
[15] G. M. Lawrence, Astrophys. J. **148**, 261 (1967).
[16] R. M. Schectman, S. R. Federman, D. J. Beideck, and D. G. Ellis, Astrophys. J. **406**, 735 (1993).
[17] Z. Delalić, P. Erman, E. Kallne, and K.-D. Zästrow, J. Phys. B **23**, 2727 (1990).
[18] E. Biémont, R. Gebarowski, and C. J. Zeippen, Astron. Astrophys. **287**, 290 (1994), and references therein.
[19] P. C. Ojha and A. Hibbert, Phys. Scr. **42**, 424 (1990).